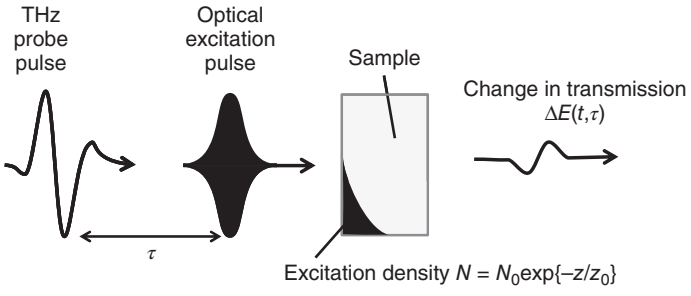

Figure 3.8 Schematic of the femtosecond-pump-tera-Hertz-probe-experiment. (Adapted after Henry *et al*. [66].)

inorganic semiconductors which emit THz pulses upon acceleration of the photo-induced carriers in an electric field or by excitation of non-linear crystals such as ZnTe. The electric field strength of the THz pulse is even lower than that of microwave radiation. The detection is done by gating the THz probe pulse with a femtosecond pulse of variable delay and with photoconductive or electro-optical sampling. It is basically the reverse of the methods used to generate THz pulses. The Fourier transformation of the pulses is used to calculate the refractive index and absorption. The complex dielectric functions can be used to obtain the complex conductivity. Again, as in TRMC, the charge generation efficiency of the organic material has to be known to obtain mobility in a time window of 1–40 ps. For a detailed description of THz spectroscopy, the reader is referred to Ref. [64].

3.3.1.7 Optical Probing

An independent and complementary method to measure the charge carrier mobility on ultra-fast time scales has recently been introduced by Devižis *et al*. [67]. It is based on time-resolved electric-field induced second harmonic generation (SHG). Any process that changes the electric field distribution in the material will affect the temporal SHG signal. In turn, the SHG intensity can be taken as a probe of changes of the electric field due to charge motion. Upon generating charge carriers in a charged capacitor by a short laser flash, the moving charge partially shields the electric field and the SHG efficiency decreases. Measuring the decrease of the SHG signal as a function of time after the laser pulse yields the time dependence of the carrier motion.

3.3.2 Carrier Transport in the Band Regime and in the Hopping Regime

Charge transport in an organic semiconductor is controlled by the transfer of an electron in the "LUMO" of a donor site to the empty LUMO of an electron accepting site. Equivalently, a hole can be transferred at the HOMO level. A *site* may be a molecule or a conjugated segment of a polymer. Electronic coupling among the sites is a necessary yet not sufficient condition for this charge transfer process to occur. In a perfectly ordered crystal at $T = 0$ K, an electron (or, equivalently a hole) would move coherently within a band of states constructed from the LUMO (or HOMO) orbitals of the constituent molecules with bandwidth 4β (cf. Section 2.4.3). When applying an electric field, a charge carrier would move at a constant mobility due to scattering at the band edge. In a molecular crystal, this condition is never met because of inadvertent structural irregularities. At finite temperature, vibrations of the lattice will scatter the charge carrier in addition. However, as long as this scattering process is only a weak perturbation to the overall coupling between the adjacent molecules, charge transport can still be described in terms of a band model. This yields a mobility that decreases with increasing temperature because the number of scattering events increases. So far we only considered the so-called *non-local coupling* between a charge carrier and low energy, that is, long wavelength, inter-molecular vibrations (*phonons*). However, at higher temperatures intra-molecular vibrations

also become important. The reason is that once adding or removing an electron to or from a molecule the distribution of the π-electrons changes (see Chapter 1). This can be expressed in terms of so-called *local phonon coupling*, considering, though, that in this case the "phonon" is a molecular vibration and the coupling is of the vibronic type (cf. Box 2.1). If the strength of this vibronic coupling becomes comparable to the electronic inter-site coupling, a band model becomes inappropriate. In the extreme case, a charge carrier is scattered at each site, that is, there is a transition from a band transport to a hopping-type motion. This is accompanied by a change of the temperature dependence of the charge carrier mobility. A further complication arises when the material is not crystalline but microscopically disordered as realized in a molecular or polymeric glass. In this case transport is controlled by (i) the electronic coupling among the constituent molecular units, (ii) the coupling to intra-molecular as well as inter-molecular vibrations, and (iii) the static intra- as well as inter-molecular disorder.

Depending on which coupling mode dominates, different transport models have been developed, such as models based on band transport, polaronic models, and models that focus on the effects of disorder. Organic solids encompass a broad class of materials, including molecular crystals, molecular glasses, and polymeric glasses. It is necessary to obtain some basic understanding on which parameters affect charge transport in order to assess which model may be suitable to describe a particular experimental situation. In order to develop such a broader view and a general qualitative understanding of charge transport, it is beneficial to consider the general one-electron Hamiltonian shown in Eq. (3.34). In this approach, we follow the outline taken in [3]. This Hamiltonian assumes a low carrier density and effects due to electron correlation or Coulomb interaction are not considered. Despite this limitation, this general one-electron Hamiltonian is useful to illustrate different limiting cases.

$$
\begin{aligned}
H &= H_0 + H_1 + H_2 + H_3 + H_4 && \text{with} \\
H_0 &= \sum_n \epsilon_n a_n^\dagger a_n + \sum_\lambda \hbar\omega_\lambda \left(b_\lambda^\dagger b_\lambda + \frac{1}{2} \right) && \text{electronic and vibrational excitation term} \\
H_1 &= \sum_{\substack{n,m \\ n \neq m}} J_{nm} a_n^\dagger a_m && \text{electron transfer term} \\
H_2 &= \sum_\lambda \sum_n g_{n\lambda}^2 \hbar\omega_\lambda a_n^\dagger a_n (b_\lambda + b_{-\lambda}^\dagger) && \text{dynamic diagonal disorder term} \\
H_3 &= \sum_{\substack{n,m \\ n \neq m}} \sum_\lambda f_{nm\lambda}^2 \hbar\omega_\lambda a_n^\dagger a_m (b_\lambda + b_{-\lambda}^\dagger) && \text{dynamic off-diagonal disorder term} \\
H_4 &= \sum_n \delta\epsilon_n a_n^\dagger a_n + \sum_{\substack{n,m \\ n \neq m}} \delta J_{nm} a_n^\dagger a_m && \text{static diagonal and off-diagonal disorder term}
\end{aligned}
\tag{3.34}
$$

where

- $a_n^\dagger$ (a_n) is the creation (annihilation) operator for an electron in an orbital of energy ϵ_n at the molecular site n.
- $b_\lambda^\dagger$ (b_λ) is the creation (annihilation) operator for an vibrational mode of energy $\hbar\omega_\lambda$.
- ϵ_n is the energy in a perfectly ordered lattice and $\delta\epsilon_n$ is its variation due to static disorder.
- J_{nm} is the electronic interaction between site m and n in a perfectly ordered lattice and δJ_{nm} is its variation due to static disorder.
- $g_{n\lambda}$ and $f_{nm\lambda}$ are dimensionless coupling constants for the electron–phonon coupling.

In Eq. (3.34), H_0 yields the total energy of a system in which the molecules are electronically and vibrationally excited. In H_0, coupling between the electronic excitation and vibrational modes is not considered. The transfer of an electron from site m to site n is given by H_1. The interaction between the electronic excitation and the intra-molecular or inter-molecular vibrations (i.e., vibrons and phonons) are included given by H_2 and H_3. This is also referred to as *polaronic effects*. Note that in the context of organic semiconductors the use of the term *polaronic* thus differs from its use in

the field of crystalline inorganic semiconductors. In H_2, the energy of the site is reduced by the interaction with the vibrational mode of energy $\hbar\omega$. In H_3, coupling to the vibration alters the transition probability amplitude from site m to n. Remember that the vibration may be of an inter-molecular or an intra-molecular kind. Static disorder effects are considered in H_4, which describes the changes to the site energy or transition probability amplitude by variations in the structure of the molecular solid.

The interactions considered in the polaronic terms H_2 and H_3 introduce *dynamic disorder*, since they are based on coupling of the electronic excitation to vibrations. In contrast, the changes to site energy and transition rate in H_4 are independent of vibrations. They are merely due to variations in the morphological structure of the film or crystal, that is, intermolecular distances and orientations, and they are thus referred to as *static disorder*. When Eq. (3.34) is written out in a matrix notation, the site energies appear on the diagonal position of the matrix, and thus energetic variations are sometimes called *diagonal disorder* while changes in the transition rate from site n to m are disguised by the term *off-diagonal disorder*. In the Hamiltonian Eq. (3.34), only linear coupling to lattice vibrations is considered. Throughout this article, the mere expression "disorder" refers to static disorder only, while we tend to employ the expression "polaronic effects" to discuss the effects due to the electron–phonon coupling expressed in H_2 and H_3.

The nature of the charge transfer is determined by the relative magnitude of the interaction energy J_{nm}, the strength of the electron–phonon coupling expressed though the coupling constants in $g^2_{n\lambda}\hbar\omega_\lambda$ and $f^2_{nm\lambda}\hbar\omega_\lambda$, and the degree of static disorder present and expressed through $\delta\epsilon_n$ and δJ_{nm}. Transport that is entirely dominated by H_1 is *band-transport*. This transport mode usually pertains to inorganic semiconductor crystals such as silicon or GaAs. *Polaronic transport* prevails if the terms H_2 and H_3 are dominant in Eq. (3.34). In the chemical and life sciences, this is better known as *Marcus-type transport*, since the pertinent equations have become popular through the treatment by Marcus [68]. If H_4 controls the mode of transport, one talks of *disorder-controlled transport*. As shall be detailed below, polaronic and disorder-controlled transport are both a form of *hopping transport* (as opposed to band transport). Having clarified some of the terminology used, we can now turn to considering different modes of charge transfer in more detail.

3.3.2.1 Band Transport

If the interaction energy with the nearest neighbor, $J_{n,\,n+1}$, is large compared to any other energy present due to dynamic or static disorder ($H_1 > H_2,\ H_3, H_4$ in Eq. (3.34)), charge transport takes place through a band. The charge carrier delocalizes as described in Section 2.4.3 to form a propagating Bloch wave that may be scattered by lattice vibrations. The charge carrier mobility is then given by $\mu = e\tau/m_{\text{eff}}$, where τ is the mean scattering time and m_{eff} is the effective mass of the charge carrier. m_{eff} is determined by the electronic coupling J. Band transport can occur only if the bands are wider than the uncertainty of the charge carrier's site energy. This requirement implies that by zero order reasoning [3] the charge carrier mobility must very roughly exceed $ea^2W/\hbar kT$, where e is the elementary charge, a is the lattice constant, and W is the band width. For organic semiconductors, $W \approx 10\,\text{kT}$ and $a \approx 0.6\,\text{nm}$ so that band transport can be considered to prevail if μ exceeds about $5\,\text{cm}^2\,\text{V}^{-1}\,\text{s}^{-1}$. The requirement of the electronic coupling being large compared to dynamic or static disorder can be fulfilled in molecular crystals at low temperature. Compared to inorganic crystals where covalent interactions prevail, electronic coupling J is weak in molecular crystals and the resulting bands are rather narrow, typically in the range of 50–500 meV [69]. The temperature dependence of the mobility in molecular crystals is experimentally found to vary as

$$\mu \propto T^{-n}, \quad 0 < n < 3 \tag{3.35}$$

and this is accounted for by theory as a result of increasing scattering with temperature by acoustic phonons, by impurities or by electron-interactions [70, 71]. The reduction of mobility with temperature as expressed in Eq. (3.35) is commonly taken as indication that band-type transport prevails.

A prototypical example of band-like transport in a molecular crystal is contained in the work of Karl and coworkers who measured electron and hole mobilities in a naphthalene crystal in the

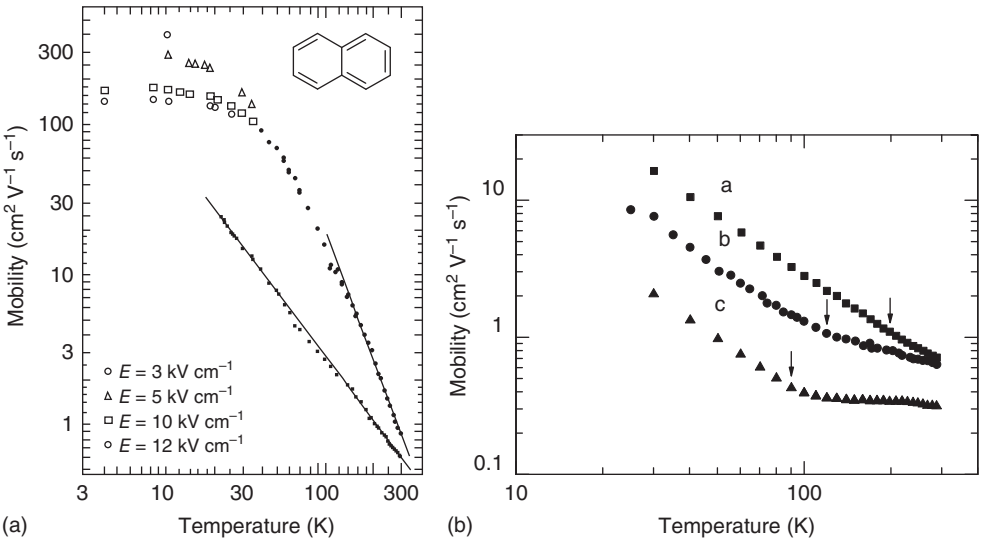

Figure 3.9 (a) The temperature dependence of the electron and hole mobilities for in an ultrapure crystal of naphthalene on a double-logarithmic scale for the applied electric fields E given in the figure parallel to the crystallographic a direction. At low temperatures, the mobilities depend on the electric field. The solid lines indicate a T^{-n} power law temperature dependence with exponents $n = 1.40$ for the electron mobility μ^- and $n = 2.90$ for the hole mobility μ^+. (Data from Warta and Karl [72].) (b) The anisotropy in the temperature dependence of the electronic drift mobility in naphthalene. Curves a–c represent different crystallographic directions. The arrows indicate the onset of deviation from the $\mu \propto T^{-n}$ dependence. (Data from Kenkre *et al*. [73].)

temperature range of 4–300 K. Figure 3.9(a) [72] shows that both electron and hole mobilities along the crystallographic a and b directions increase with decreasing temperature featuring a $\mu \propto T^{-n}$ law with exponents of 2.9 (holes) and 1.42 (electrons). Below 30 K the hole mobilities level off and saturate at values of the order of 200 $cm^2\ V^{-1}\ s^{-1}$ depending on the electric field. It is worth remembering that it took Karl and his coworkers more than a decade to improve the techniques for material purification and crystal growth in order to eliminate trapping effects that would otherwise obscure intrinsic transport at temperatures as low as 4 K. The results unambiguously prove that at temperatures below 300 K charge transport is band-like.

When measuring electron transport in a naphthalene crystal along the three crystallographic directions, a pronounced anisotropy is noted (Figure 3.9(b)) ([73] Figure 3.2). At 20 K, the mobility measured along the crystallographic direction perpendicular to the ab-plane (usually designated as c'-direction) is one order of magnitude lower than that along the a-direction. This reflects the anisotropy of the transfer integrals J inferred from DFT calculations. It is also remarkable that the lower the band-type mobility is, the earlier $\mu(T)$ deviates from the $\mu \propto T^{-n}$ dependence when raising the temperature. This is a signature of the breakdown of the band concept to describe transport. It indicates that now phonon coupling is no longer a weak perturbation of coherent band transport but competes with the electronic exchange interaction. A consequence of this phonon coupling is that the transport bands shrink and the effective mass of charge carriers increases. Evidence for this band narrowing with increasing temperature is documented by angle and energy resolved UV photoelectron spectroscopy on thin crystalline pentacene film deposited on graphite. Such experiments reveal the valence band structure and show that the bandwidth in the a direction ([100] direction) indeed decreases from 240 meV at 140 K to 190 meV at 300 K [74].

Unfortunately, in many molecular crystals the mobilities measured at or near room temperature are of the order of $1\,cm^2\,V^{-1}\,s^{-1}$, indicating that there is a cross-over between band and hopping motion (see below). Exceptions are crystalline rubrene [75] and perhaps pentacene because of the comparatively large electronic inter-molecular coupling. This is a challenge for establishing an adequate theoretical concept because perturbation approaches fail. A further complication toward a unified theoretical formalism is that the conventional polaron hopping approach (detailed below) is based upon non-local phonon coupling and, even worse, it is restricted to low frequency modes ($\hbar\omega_o \ll kT$). Thus, it neglects the contribution of intra-molecular vibrations. Both assumptions are serious oversimplifications. Their reconsideration is the subject of more recent research [76–78]. For further details, the reader is referred to the review article by Coropceanu *et al*. [69].

3.3.2.2 Hopping Transport

If any of the other energies due to the effects of dynamic or static disorder become significant compared to the nearest neighbor interaction energy ($H_1 < H_2,\ H_3, H_4$ in Eq. (3.34)), the transport band made up of delocalized wavefunctions is destroyed. In this case, transport can no longer be described in terms of band motion but rather becomes incoherent. Then, a charge carrier is localized at individual sites and proceeds by a sequence of non-coherent transfer events. This is referred to as *hopping* motion. This is similar to the case of excitons, where one can have a coherent transfer mode via a delocalized Frenkel exciton and a non-coherent mode via exciton hopping. A transport band can be destroyed because of too much geometric relaxation when the carrier gets onto the molecule (H_2), too much vibration (H_3), or too much initial variation in site energy or inter-site distance (H_4).

3.3.2.3 Polaronic Transport

In the context of molecular crystals, polaronic transport has been pioneered by Austin and Mott [79], Holstein [80, 81], and Emin [82]. The resulting transport mechanism is equivalent to that suggested by Marcus for electron transfer from one molecule to another in solution [68, 83]. Consider the situation of a perfectly ordered crystal where electronic coupling among the transport sites, that is, the HOMOs or LUMOs of adjacent molecules, is very small compared to the electron–phonon coupling ($H_1 \ll H_2, H_3$; and $H_4 = 0$). In this case, a charge carrier is localized at a given site due to dynamic disorder. As the charged molecule couples to the surrounding molecules inter-molecular displacements and polarization effects alter the van der Waals energy between the molecules. The charge thus forms a (*small*) *polaron*. Transport occurs via inter-site polaron hopping. As illustrated in Figure 3.10, the transfer of the charge is associated with a distortion of the molecule and its environment, which requires *reorganization energy* λ. As a result, the transfer process becomes thermally activated. The reorganization energy consists of two contributions, $\lambda = \lambda_{inner} + \lambda_{outer}$. One term is called the *inner reorganization energy*, λ_{inner}, because it is associated with the intra-molecular distortion occurring when a molecule becomes charged. The change in molecular energy due to inter-molecular displacement and polarization is called the *outer reorganization energy*, λ_{outer}. In electron transfer reactions in aqueous solutions, the latter term is important, because solvation effects are strong. In rigid organic solids, however, molecular displacements are very small or even negligible. Consequently, the inner reorganization energy is dominant. As illustrated in Figure 3.10, the inner reorganization energy λ_{inner} for a transfer of charge from molecule A to B consists of the sum of the relaxation energies λ_A and λ_B for molecule A and B, respectively, that is, $\lambda_{inner} = \lambda_A + \lambda_B$.

In the context of molecular crystals, the energy difference between a molecule without the distortion caused by an additional electron and that with the distortion is also known as the *polaron binding energy* E_{pol} (Figure 3.11). Austin and Mott [79] demonstrated that half the polaron binding energy is what is needed as activation energy for transport. We briefly summarize the key points of their treatment. Consider two identical molecules 1 and 2 with intra-molecular normal mode coordinates Q_1 and Q_2 and define their potential energies such that $E_1(Q_1 = 0) = E_2(Q_2 = 0) = 0$. The potential energy of the neutral molecules as a function of its normal mode coordinate is then $E_1(Q_1) = AQ_1^2$ and $E_2(Q_2) = AQ_2^2$. An additional electron that is placed on molecule 1 distorts the molecule. Assuming

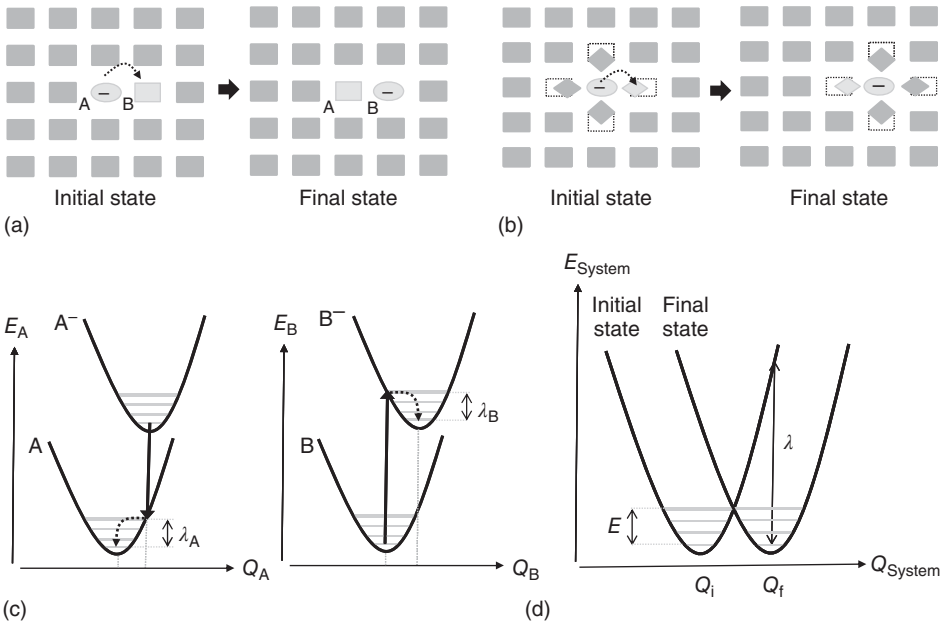

Figure 3.10 Illustration of charge transfer in a perfectly ordered molecular crystal. The transfer of a charge from molecule A to B is associated with a change (a) in the geometry of the molecules A and B themselves (expressed graphically by changing shapes) and (b) in the position and geometry of the molecules surrounding the charged molecule. The former gives rise to the inner reorganization energy λ_{inner}, the latter causes the outer reorganization energy λ_{outer}. (c) The inner reorganization energy λ_{inner} is composed of the relaxation energies λ_A and λ_B, $\lambda_{inner} = \lambda_A + \lambda_B$. λ_A is the energy associated with the change in molecule A from the equilibrium geometry of the charged state to that of the ground state immediately after the charge had been transferred onto B. Similarly, λ_B is the energy associated with the change in B^- from the ground state equilibrium geometry to the charged state equilibrium geometry, immediately after accepting the charge. (d) To describe the transfer, it is more helpful to consider the potential energy of the entire system (molecule A, B, and surrounding molecules) as a function of a generalized configuration coordinate describing the entire system. If the charge is on A, the system is described by the "initial state" curve with a minimum at Q_i. The "final state" curve with minimum at Q_f describes the energy of the system and its dependence on the geometry when the charge is on B. The reorganization energy λ gives the difference in potential energy when the system is at Q_f (=charge on B) instead of Q_i (charge on A). It is the sum of outer and inner reorganization energy. The transfer of a charge from A to B does not require the full value of λ. Rather, it can take place either by quantum mechanical tunneling from Q_i to Q_f or by thermal activation with an energy $E = \lambda/4$ to the point where initial and final state potential energy curves cross. The latter is the key idea of *Marcus' Theory*.

only small distortions, the associated energy depends linearly on the molecular distortion, that is, it is $-BQ_1$. The energy of molecule 1 with a charge on it therefore becomes $E_1(Q_1) = AQ_1^2 - BQ_1$, and the minimum of the parabolic potential is shifted to a new equilibrium coordinate Q_0. It is found by $dE_1(Q_1)/dQ_1 = 0$ and it is $Q_0 = B/2A$. The associated equilibrium energy of the charged molecule is $E_1(B/2A) = -B^2/4A = -AQ_0^2$. This is the value of the polaron binding energy E_{pol}.

If the polaron jumps from a site 1 to site 2, the potential energy curves must cross. By simply geometry one can show that the energy neededе to distort the molecule from its equilibrium geometry to that of the crossing point is $E_{min}^{reorg} = (1/2)AQ_0^2 = (1/2)E_{pol}$. The probability per unit time that an electron jumps from one molecule to another, identical molecule is thus proportional to $\exp(-E_{min}^{reorg}/kT)$, and the activation energy inferred from the temperature dependence of the jump rate is therefore half

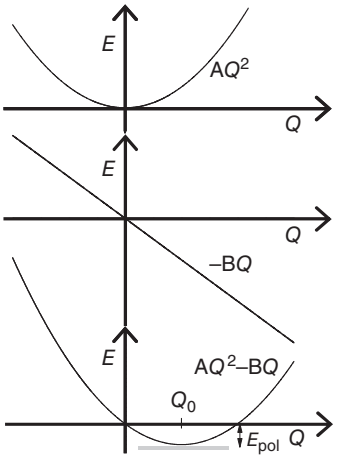

Figure 3.11 (a) The (electronic) potential energy $E = AQ^2$ of a molecule as a function of a configuration coordinate Q in the harmonic approximation, with the equilibrium position of the configuration coordinate set to 0. (b) The additional (electronic) potential energy $E = -BQ$ that results from a change in the configuration coordinate such as compression/elongation of a bond or torsion/planarization of an angle, presuming linear coupling of the electronic energy to the configuration coordinate. (c) When the linear coupling of the electronic energy to the molecular distortion is added to its usual quadratic dependence to give $E = AQ^2 - BQ$, a new equilibrium position Q_0 of the configuration coordinate that is associated with an lower potential energy results. The difference in electronic energy with and without the linear coupling term is the polaron binding energy E_{pol}. (After Austin and Mott [79].)

of the polaron binding energy, that is, $(1/2)E_{pol}$. When comparing the Austin and Mott-type treatment with the Marcus-type picture of Figure 3.10, it is evident that $E_{min}^{reorg} = (1/2)E_{pol} = \lambda/4$, that is, the activation energy for transport is half the polaron binding energy and a quarter of the reorganization energy λ.

The conceptual approach for polaron hopping has been laid down in the seminal paper by Holstein [80, 81]. Of course, if the electronic transfer integral was exactly zero, a charge carrier would not move at all. However, weak electronic coupling can be introduced in the Holstein formalism as a perturbation. In the classical limit, it is assumed that the phonon energy is small compared to the thermal energy kT. This yields a hopping rate

$$k_{ET} = \frac{J^2}{\hbar}\sqrt{\frac{\pi}{2E_{pol}kT}}\exp\left(-\frac{E_{pol}}{2kT}\right) \tag{3.36}$$

where J is the transfer integral. Noting that E_{pol} is half of the reorganization energy, Eq. (3.36) is identical to the Marcus equation in electron transfer reactions (Box 3.5). From Eq. (3.36), the mobility of a charge carrier can be derived by considering that the mobility μ relates to the diffusion constant D via the Einstein relation, $\mu = eD/kT$, and the diffusion constant is determined by the hopping rate through $D = (1/2n)k_{ET}a^2$ where n is the dimensionality of the crystal and a is the distance between lattice sites. For a three-dimensional system with $n = 3$, one obtains

$$\mu = \frac{ea^2J^2}{6\hbar(kT)^{\frac{3}{2}}}\sqrt{\frac{\pi}{2E_{pol}}}\exp\left(-\frac{E_{pol}}{2kT}\right) \tag{3.37}$$

Equation (3.37) predicts an Arrhenius-type temperature dependence for μ, except when $E_{pol}/2kT \ll 1$, where the pre-exponential $T^{-3/2}$ dependence takes over. For a realistic value of 100 meV for E_{pol} the temperature at which $\mu(T)$ merges into a $T^{-3/2}$ dependence is above 600 K. This

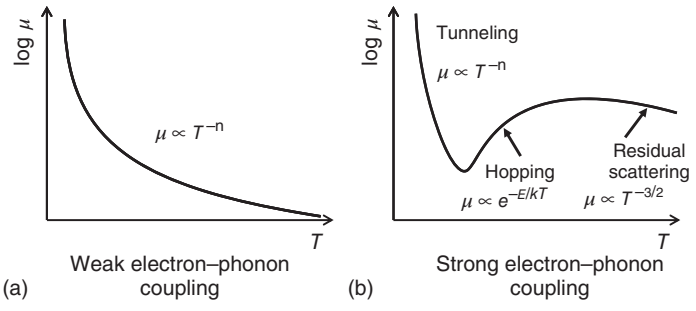

Figure 3.12 The type of temperature dependence of the charge carrier mobility predicted by the Holstein polaron model in the case of weak (a) and strong (b) electron–phonon coupling.

implies that one should be cautious with the custom of approximating the mobility by

$$\mu = \mu_0 \exp\left(-\frac{E_{\text{pol}}}{2kT}\right) \tag{3.38}$$

and determining the *prefactor mobility* μ_0 by extrapolating a $\log \mu(T)$ versus $1/T$ plot to infinite temperature.

In cases where the phonon coupling is weak and the temperature is low ($T < 300\,\text{K}$), the mobility is controlled by band-type transport. As the temperature increases, there is a superposition of the (decreasing) contribution of band motion and increasing thermally activated hopping. Eventually the latter takes over and, concomitantly, $\mu(T)$ passes through a minimum. Finally, $\mu(T)$ will approach a $T^{-3/2}$ law. This is illustrated in Figure 3.12 ([69]).

Box 3.5 Marcus Theory for Electron Transfer

Marcus was awarded with the Nobel prize for his contributions in describing electron transfer from a donor molecule to an acceptor molecule in solution [68, 83, 84]. The basic idea of classical Marcus theory can be summarized by considering two identical, isoenergetic molecules in a solvent (Figure B3.5.1). The electron donating molecule, the accepting molecule and the solvent are considered a system that can be described by a generalized configuration coordinate Q and an associated potential energy curve that is approximated as a parabola. In the initial state, with the electron still on the donor molecule, the potential energy of the system has a minimum at Q_i. In the final state, when the electron has transferred onto the acceptor, the system's energetic minimum occurs at Q_f. The energy needed to rearrange the initial system such that it matches the final geometry is reorganization energy λ. For electron transfer to occur, it is not necessary that the initial system distorts to that extent. Rather, electron transfer already occurs at the intersection of both potential energy curves. By virtue of them being equal parabolas, this intersection can be reached with an activation energy of $\lambda/4$, which can be provided by thermal fluctuations, that is, excitations of (internal or external) phonons. Fluctuations in the vibrational coordinates (internal phonon modes) need to be considered when equilibrium bond lengths or angles change between the initial and final state of the donor or acceptor. In addition, fluctuations in the orientational coordinates of the solvent molecules (external phonon modes) are particularly important in polar solvents. The rate constant for electron transfer then depends on the probability of reaching the intersection (giving rise to an exponential factor with an activation energy E_a), a frequency for crossing attempts (e.g., collision frequency), and the probability for crossing the surface (such

as the transmission coefficient). In a semiclassical approach, starting with Fermi's golden rule, the collision frequency and transmission coefficient are implicitly included in the electronic coupling J. The rate of electron transfer between identical, isoenergetic molecules is then

$$W = \frac{J^2}{\hbar}\sqrt{\frac{\pi}{\lambda kT}}\exp\left(-\frac{\lambda}{4kT}\right) \tag{B3.5.1}$$

Classical Marcus theory appears mathematically as the high-temperature limit of Holstein's small polaron theory, with $E_{\mathrm{pol}} = \lambda/2$ and, for isoenergetic sites, with $E_{\mathrm{a}} = \lambda/4 = E_{\mathrm{pol}}/2$. While Marcus treated electron transfer between individual molecules in solution, Holstein considered electron transfer in a molecular crystal [81, 86]. In Marcus theory, one can account for a difference in potential energy between the initial state (=electron on the donor) and the final state (=electron on the acceptor) by including the term ΔG^0 in the activation energy, thus leading to the form

$$W = \frac{J^2}{\hbar}\sqrt{\frac{\pi}{\lambda kT}}\exp\left[-\frac{\lambda}{4kT}\left(1+\frac{\Delta G^0}{\lambda}\right)^2\right] = \frac{J^2}{\hbar}\sqrt{\frac{\pi}{\lambda kT}}\exp\left[-\frac{\left(\lambda+\Delta G^0\right)^2}{4\lambda kT}\right] \tag{B3.5.2}$$

Equations (B3.5.1) and (B3.5.2) are valid when the energy of internal and external phonons are small compared to the thermal energy of the environment, $\hbar\omega \ll kT$. Marcus theory has been confirmed by many experiments. Note that Eq. (B3.5.3) predicts the rate of energy transfer to first increase with ΔG^0 and then to decrease. The latter is referred to as *Marcus inverted regime*. It arises because with increasing ΔG^0 the point of intersection between both potential energy curves first lowers, then passes through zero and then raises again as can be seen when shifting the two parabolas vertically. The inclusion of an energy difference between the initial and the final states of the system in Marcus theory is equivalent to including the effects of energetic disorder in a (Holstein) polaron model. This shall be discussed further in Section 3.3.2.5.

The classic approach of Eqs. (B3.5.1) and (B3.5.2) is no longer suitable when tunneling between the initial and final state needs to be taken into account. This can be the case for large energy differences between the initial and final states, and, in particular, for electron transfer at low temperatures. In this case, the average external phonon modes are still small compared to kT, yet the internal phonon modes become comparable or even large. As a result, the external phonon modes and the external reorganization energy λ_0 can still be treated classically. However, an average internal (=high-frequency) phonon mode $\hbar\omega$ with associated Huang–Rhys factor S is incorporated in a quantum chemical fashion. The corresponding mathematical equation [87–89] for the rate constant of electron transfer is often referred to as *Marcus–Levich–Jortner expression*.

$$W = \frac{J^2}{\hbar}\sqrt{\frac{\pi}{\lambda_0 kT}}\sum_{n=0}^{\infty} e^{-S}\frac{S^n}{n!}\exp\left[-\frac{\left(\lambda_0+\Delta G^0+n\hbar\omega\right)^2}{4\lambda_0 kT}\right] \tag{B3.5.3}$$

At very low temperatures when both, internal and external phonon modes become comparable to kT, Eq. (B3.5.3) no longer applies since both type of vibrations need to be treated quantum chemically. For this case, Lanzani [90] gives an expression for the energy transfer rate as

$$W = \frac{2\pi J^2}{\hbar\omega_{\mathrm{S}}}\sum_{n=0}^{\infty}\mathrm{e}^{-(S_{\mathrm{S}}+S)}\frac{S_{\mathrm{S}}^{p(n)}}{p(n)!}\frac{S^n}{n!} \tag{B3.5.4}$$

where the index S specifies the external, solvent-related quantities and $p(n)$ is the average number of solvent phonon modes involved in the transition.

Marcus theory has been confirmed experimentally [85, 91]. When deviations seem to occur between Marcus theory and the transfer rates measured in solution it is worth checking whether the transfer reaction has inadvertently become diffusion-limited instead of reaction-limited [91].

For further information concerning Marcus theory, we refer the reader to [90–95].

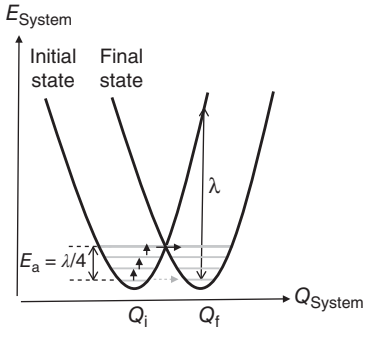
E_{System}
Initial state
Final state
λ
$E_a = \lambda/4$
Q_{System}
Q_i
Q_f

(a)

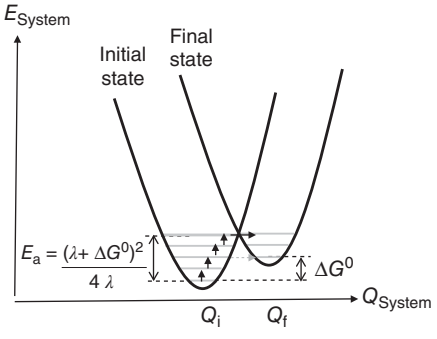
E_{System}
Initial state
Final state
$E_a = \frac{(\lambda + \Delta G^0)^2}{4\lambda}$
ΔG^0
Q_{System}
Q_i
Q_f

(b)

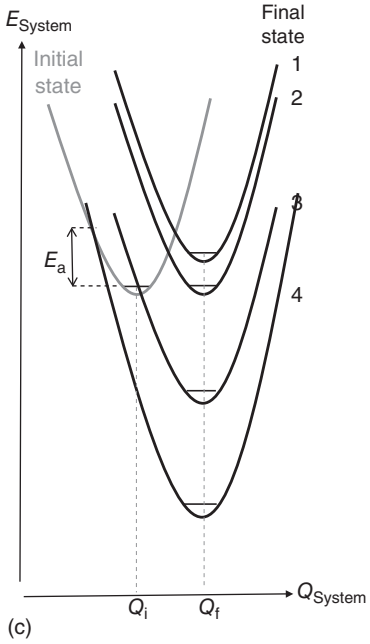
E_{System}
Initial state
Final state
1
2
3
4
E_a
Q_{System}
Q_i
Q_f

(c)

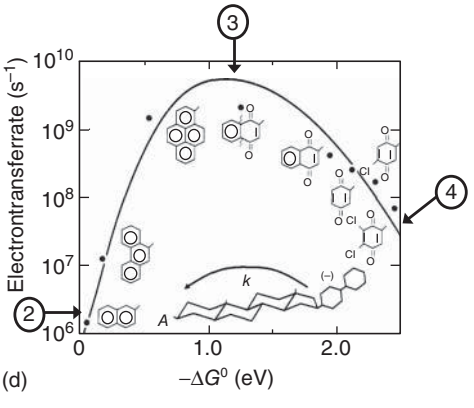
3
4
2
Electrontransferrate (s^{-1})
10^{10}
10^9
10^8
10^7
10^6
0
1.0
2.0
$-\Delta G^0$ (eV)
k
A
(–)
Cl

(d)

Figure B3.5.1 Illustrating of Marcus theory of electron transfer. (a) Potential energy diagram showing the energy of the entire system (donor, acceptor, and solvent) in the initial state and in the final state as a function of a general configuration coordinate Q_{System}. Transfer from the initial to final state can occur at the point where the two potential curves intersect. This requires thermal, that is, vibrational activation to deliver an energy $E_a = \lambda/4$. In a quantum mechanical treatment, tunneling between the potential minima of both states may be included (gray arrow). (b) If the energy of the final state is displaced by ΔG^0 compared to the initial state, a correspondingly higher activation energy is needed. The process of tunneling in a quantum mechanical treatment requires phonon activation (gray arrow). (c) The rate of transfer depends exponentially on the energy difference to the intersection point of the parabolas, that is, it is $\propto \exp(-E_a/kT)$. When the energy of the final state reduces as shown for parabolas 1–3, the activation energy for transfer first decreases (*Marcus normal regime*), then, as seen for parabola 4, it increases again (*Marcus inverted regime*). (d) The electron transfer rate as a function of $-\Delta G^0$ measured by Miller *et al*. [85] for intramolecular electron transfer for the molecules shown as inset, that is, from a biphenyl via the spacer shown to the various acceptor moieties, dissolved in MeTHF. With increasing energy offset, the transfer rate accelerates by more than three orders of magnitude, reaches a maximum and reduces again. The numbers refer to the corresponding parabola sketched in (c). The maximum is reached for a value of $-\Delta G^0 = 1.2\,\text{eV}$. The solid line is calculated following Eq. (B3.5.3) below, using $\hbar\omega = 1500\,\text{cm}^{-1}$ and including contributions of a solvent reorganization energy of $\lambda_0 = 0.75\,\text{eV}$ and a reorganization energy $S \cdot \hbar\omega$ for the internal vibrational modes of 0.45 eV.

3.3.2.4 Disorder-Controlled Transport

Most organic semiconductors used in devices are noncrystalline, implying that variations in the site energy $\delta\epsilon_n$ and in the distance between sites, and, concomitantly, in the intermolecular coupling δJ_{nm} are large compared to the value of intermolecular coupling energy J_{nm} ($H_1 \ll H_4$ in Eq. (3.34)). This has a considerable impact on the mobility of charge carriers. It implies that charge transport occurs as a random walk by incoherent hopping between neighboring transport sites. The charges are localized onto the sites because of static disorder. If a system is perfectly ordered and hopping transport results only from dynamic disorder (perfect polaronic transport), then charge transport is controlled by a well-defined thermally activated hopping rate that determines diffusivity and mobility of the charges via the Einstein relation between their diffusivity and mobility as outlined in the preceding section. In that case, diffusivity and mobility are time-independent. In contrast, in disordered materials the situation is more complicated because the sites are neither equally spaced nor isoenergetic. This implies that the jump rates are asymmetric. Forward and backward jumps have different activation energies, quite in contrast to the polaronic case. Transport is controlled by the occupational probability, p_i, of any site of the system, with the sites (representing chromophores) differing in energy and inter-site spacing. The transport can be described by a general hopping equation of the form [96],

$$\frac{\mathrm{d}p_i(t)}{\mathrm{d}t} = \sum_{j\neq i}[-w_{ij}p_i(t)[1-p_j(t)] + w_{ji}p_j(t)[1-p_i(t)]] \tag{3.39a}$$

where $p_i(t)$ and $p_j(t)$ are the (time-dependent) probabilities that sites i and j are occupied, respectively. They become time-independent, that is, constant, once the equilibrium condition $\mathrm{d}p_i(t)/\mathrm{d}t = 0$ is fulfilled. w_{ij} and w_{ji} are the hopping rate from site i to j and vice versa. Equation (3.39a) accounts for any density of charges in the DOS. It is thus particularly suited to describe charge transport in OFETs or SCLC in OLEDs, where charge carrier densities are significant. In the limit of low charge carrier densities, for example, when describing the motion of charges generated in a TOF experiment, one can use the approximation $p_i p_j \approx 0$. Equation (3.39a) then reduces to

$$\frac{\mathrm{d}p_i(t)}{\mathrm{d}t} = \sum_{j}[-w_{ij}p_i(t) + w_{ji}p_j(t)] \tag{3.39b}$$

Frequently, the lifetime of a charge is not infinite. Rather, losses can occur with a rate λ_i. For example, such a loss process can be if an electron in a diode structure reaches the electrode and recombines there with a hole. This can be incorporated into the master equation as [97]

$$\frac{dp_i(t)}{dt} = \sum_j [-w_{ij}p_i(t) + w_{ji}p_j(t)] - \lambda_i p_i(t) \tag{3.39c}$$

Equation (3.39) has to be solved either analytically or numerically and the solution has to be averaged over all possible realizations of it. An alternative way to describe the disorder transport is using a Monte Carlo simulation.

A simple concept to explain charge carrier mobility in a disordered organic solid on a microscopic level is the *Gaussian disorder model* (*(GDM)*, also known as *Bässler model*, [98, 99]) and its subsequent extensions. It is based upon the notion that charge carriers hop within a manifold of sites that feature a Gaussian energy distribution and a Gaussian distribution of inter-site spacing. We shall introduce here the DOS and the hopping rate that may be incorporated in the model and present the basic elements of the formalism.

The Density of States (DOS) As detailed in Section 2.4.2, the energy levels of molecules in an amorphous film characterized by randomly varying intermolecular distances are described by a Gaussian distribution, $g(\varepsilon) = (1/\sqrt{2\pi}\sigma)\exp(-(\varepsilon - \varepsilon_0)^2/2\sigma^2)$, where ε here is the energy of an individual molecule, and the standard deviation σ (the "disorder parameter") characterizes the width of the Gaussian distribution. This distribution results mainly from the van der Waals coupling with the neighboring sites. For conjugated polymers, there is an additional contribution due to the variation in the lengths and thus the energies of the conjugated segments of the chain. It is important to recognize that the broadening of DOS expressed through the value of σ is a result not so much of the magnitude of intermolecular interactions but rather of their randomness. For instance, when studying the hole mobility of hole-transporting molecules such as TAPC molecules embedded as dopants in a matrix, one finds that the hole mobility decreases by two orders of magnitude when the nonpolar polystyrene matrix is replaced by a polar polycarbonate matrix. The reason is that the random orientation of the dipole moments on the carbonyl groups roughens the energetic landscape [100, 101]. The effect vanishes if the dipole moments are topologically aligned, for example, in the case in a molecular crystal composed by polar molecules.

The fact that the DOS distribution is of Gaussian shape is straightforward because the interaction energy of a charged chromophore imbedded in an amorphous polarizable environment depends on a large number of coordinates and interactions, each varying statistically. Based upon the central limit theorem this leads to a Gaussian envelope function. This applies also to neutral excitations (excitons). In this case, the Gaussian DOS is amenable by absorption and photoluminescence (PL) spectroscopy as detailed in Chapter 2. For charged molecules, the DOS distribution cannot be assessed optically since there is no direct optical transition from the neutral to the ionized state. Instead one has to rely on electrical probing. Using an electrochemically gated transistor Hulea *et al.* [102] were able to scan the DOS distribution of a PPV film by controlled variation on the hole injection barrier from the electrolyte and the film. The experiments confirm that the center of the DOS distribution is indeed of Gaussian shape but the tail has a more complex structure. This tail is not an intrinsic property of the PPV film but is due to counter ions (ClO_4^- or PF_6^-) incorporated in the film during doping to ensure the overall film neutrality. Those ions give rise to long-range Coulomb potential fluctuations and, concomitantly, to deep states with an almost exponential trap distribution superimposed onto an intrinsic Gaussian DOS distribution [103]. As demonstrated by calculations, this effect becomes already noticeable at a dopant concentration exceeding 10^{17} cm^{-3} (Figure 3.13). To calculate the DOS distribution based upon first principles taking into account the charge distribution within the hopping sites, the anisotropic polarizabilities, and molecular packing is a theorist's dream. While there is significant progress toward this challenging goal, so far quantitative agreement with experiment still requires further work [104, 105].

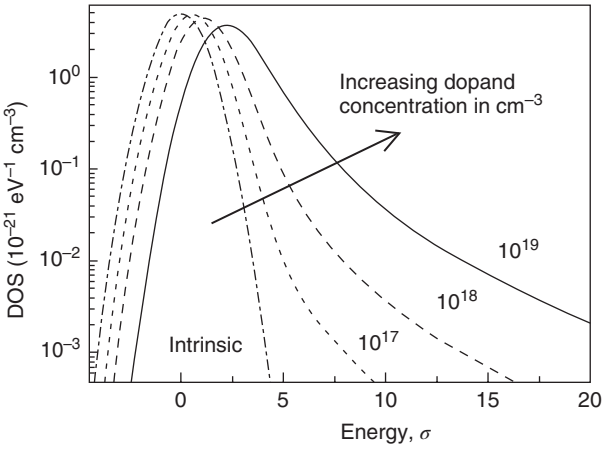

Figure 3.13 The effect of doping on the density of states distribution in a disordered organic semiconductor at variable concentration of charged dopants. The energy scale is normalized to the width of the DOS, expressed through σ, of the undoped sample ($\sigma = 80$ meV). The calculation is for an intrinsic site concentration of 10^{21} sites cm^{-3} and a dielectric constant of 3. (Data from Arkhipov *et al*. [103].)

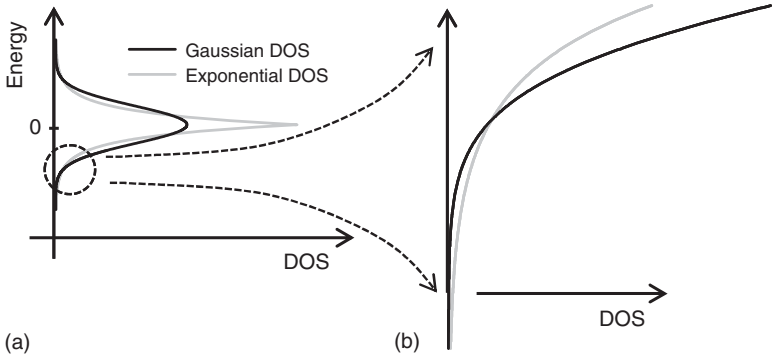

Figure 3.14 Comparison between a Gaussian and an exponential DOS with the same site concentration (a) for the full energy range of the DOS and (b) zoomed in to the tail states. Notice that the Gaussian DOS tails off faster as a function of the site energy than an exponential DOS. While here the exponential DOS is drawn symmetrically centred at zero, in a real system, of course, only the part below zero is considered to describe the tail states of a band. Note that the integral DOS in both cases is comparable.

The Gaussian DOS is sometimes approximated by an exponential function in order to facilitate the mathematical treatment, in particular when integrals are involved (Figure 3.14). While this can be a reasonable approximation for an intermediate energy interval, the infinitely long tail of the exponential function is a poor match at low energies. This creates artifacts when describing charge transport at long timescales when carriers relax to the bottom of the DOS.

In the original Bässler model (GDM), any correlation between the energies of the hopping sites had been disregarded. In a real world specimen, however, correlation can be expected. Consider a site M with a comparatively large van der Waals coupling to its neighbors. This may perhaps be due to a local compression, or due to a particular orientation of polar neighbors. Molecules adjacent to site M will find themselves in a related, similar environment and will thus be similarly affected. As a result, the energies of adjacent sites are correlated. For example, if the energetic disorder results

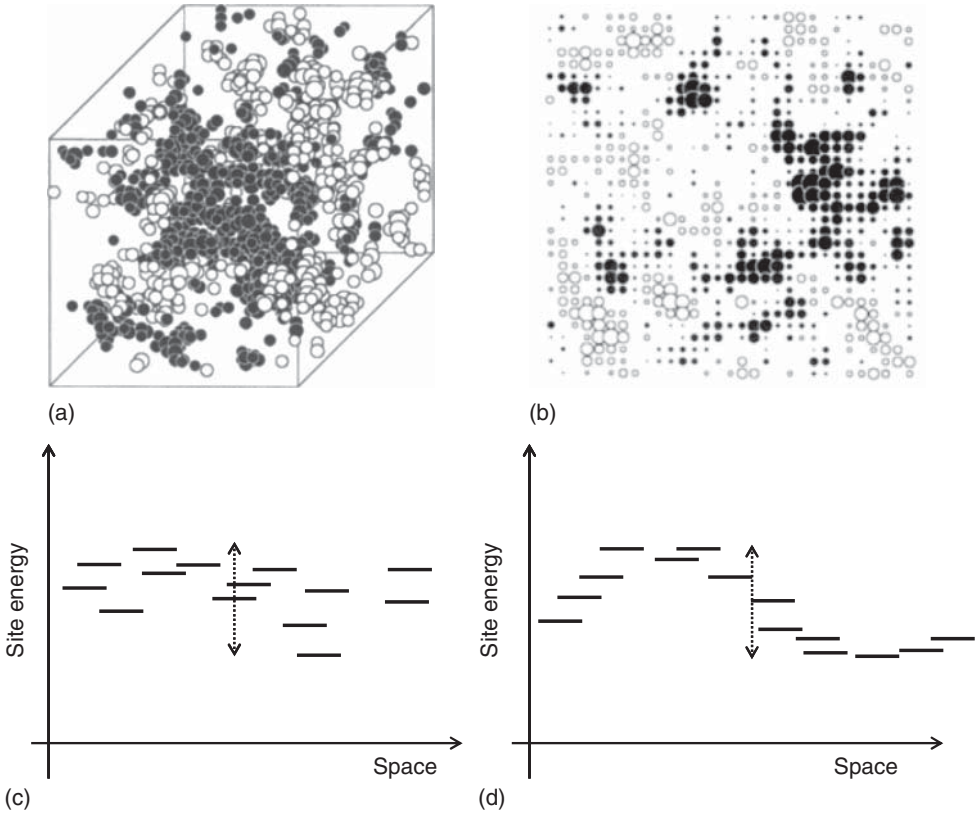

Figure 3.15 Illustration of correlated disorder. (a) Positive and negative variations of the site energy from the mean value are indicated by black and white spheres, with the radius corresponding to the magnitude of the deviation in a three-dimensional view and (b) as a two-dimensional cross section. (After Novikov and Vannikov [107].) (c) The variation of site energy with space shown for uncorrelated disorder and (d) for correlated disorder. The spread of values, indicated by the dashed arrow, is identical in both cases.

from the interaction of a charge with random permanent dipoles, the three-dimensional correlation function for the site energy is $f(r) \sim \sigma^2 a/r$, that is, it decays slowly with intersite separation r [106]. Here, σ characterizes the energetic disorder and a is the charge-dipole separation. The strong correlation of the site energy in an ensemble of uncorrelated dipoles has its origin in the long-range nature of the dipole electrostatic potential. The fall-off with distance is faster for lower dimensions – for a 2D lattice, $f(r) \sim 1/r^3$ and for a 1D lattice, $f(r) \sim (\log r)/r^3$ [107] – and for the case of a charge interacting with induced dipoles (instead of permanent ones) [21, 108]. The energy landscape that results when correlations are included can be considered as one in which a larger-scale variation of the potential energy superimposes on small local site energy fluctuations. This is equivalent to a hierarchical flattening of larger-scale energetic structures without changing the global standard deviation of the DOS distribution. An illustration of this is given in Figure 3.15. The amended version of the GDM that includes the effect of site correlation is referred to as the *correlated disorder model (CDM)*. At high electric fields, the GDM and CDM models converge. Differences arise when describing the motion of charges at low electric fields, in particular when the molecules carry some permanent dipole moment. For fields below about 1×10^5 V cm^{-1}, correlation needs to be included to arrive at a description true to experiment. Correlation effects are less important in non-polar materials, at high electric fields or when considering the motion of (neutral) excitons. The high computational expense

in Monte-Carlo simulations and the added complexity in analytical calculations are the main reason why energy correlation is not routinely taken into account.

The Hopping Rate In the case of polaronic transport between identical molecules, here is no difference between a forward jump from site i to site j and the backward jump from site j to site i. Both sites are isoenergetic and have the same polaronic binding energy. In consequence, the associated hopping rate, Eq. (3.36) is the same for the forward and backward jump. The symmetric nature of the polaronic jump rate is also evident in Eq. (B3.5.1) (in Box 3.5). When introducing static energetic disorder, this symmetry is broken. If the forward jump is downhill in energy, the backward jump is evidently uphill, and vice versa. This requires an asymmetric jump rate. A simple approach is to consider that for the downhill direction, excess energy is simply dissipated while for the uphill transfer, an activation energy is required in the form of a Boltzmann factor. This introduces an energy dependence that needs to be multiplied with the transfer rate due to the electronic coupling between the two sites. In general, this coupling may be approximated as a dipole coupling (with a rate proportional to $(r_0/r_{ij})^6$, r_0 being a constant, r_{ij} being the distance between sites i and j), or an exchange coupling (with a rate following $\exp(-2\gamma r_{ij})$) may be considered. The use of dipole coupling can be appropriate to describe the incoherent hopping of excitons in a disordered medium. When describing charge transport, coupling occurs by exchange. This is expressed through the hopping rate w_{ij} of Miller and Abrahams (*MA model*) [109]

$$w_{ij} = \nu_0 \exp(-2\gamma r_{ij}) \times \begin{cases} \exp\left(-\frac{\varepsilon_j - \varepsilon_i}{kT}\right), & \varepsilon_j > \varepsilon_i \\ 1, & \varepsilon_j \leq \varepsilon_i \end{cases} \tag{3.40}$$

where r_{ij} the jump distance between sites i and j, and γ is the inverse localization radius of the electron wavefunction. It is related to the electronic coupling matrix element between adjacent sites. ν_0 is a frequency factor (*attempt-to-hop frequency*). Equation (3.40) implies that the hopping sites are point sites, neglecting that the dielectric coupling can depend on the mutual orientation of the transport molecules. The MA model assumes that the Boltzmann factor is equal to 1 for a downward jump regardless of electric field and that there is always an energy accepting phonon mode available to dissipate the excess energy released when a charge carrier hops to a lower energy site. In contrast, thermal activation is required for a jump to a site at higher energy.

When the Gaussian DOS is used together with an MA rate in order to account for charge transport, one obtains a model that is purely disorder-based without any contributions from polaronic effects. In the language of the Hamiltonian of Eq. (3.34) chosen for illustration, this would correspond to the case $H_1 \ll H_4$ and $H_2 = H_3 = 0$, (with $\delta\epsilon_n$ varying statistically and a variation in δJ_{nm} resulting from a positional disorder). Note that such an approach ignores the need for geometric reorganization energy when a molecule becomes charged. This limitation is eliminated when using Marcus-type hopping rates, so that polaronic effects are included. The superposition of disorder and polaronic effects is the concern of the next section, Section 3.3.2.5. We shall first consider the formalism for and the results obtained with a purely disorder-based model.

The Formalism To proceed from a microscopic description of charge transfer between the chromophores of an amorphous organic semiconductor to a macroscopic description that yields the macroscopic mobility requires ensembles averaging. This is the most difficult task.

The easiest way to accomplish this is by using a Monte Carlo (MC) simulation. The MC simulation can be considered an idealized computer-based experiment that is carried out under well-defined starting conditions on a virtual sample that has an arbitrarily adjustable degree of disorder. It not only tells you which degree of sophistication is needed for reproducing the behavior of a real-world sample but also allows you to check the validity of approximations that are inevitably involved in an analytic theory.

The first analytic treatment of hopping transport in an amorphous solid with a Gaussian DOS distribution was based upon an *effective medium approach* (*EMA*) [97, 98, 110]. This analytic

treatment allows portraying how an ensemble of independent particles evolves as a function of energy within in the DOS distribution. The "particle" can either be a charge carrier or be a neutral singlet or triplet excitation. It turns out that for an undiluted system such as an amorphous molecular film, this theory describes the hopping process in a satisfactory way except at low temperatures when intermediate thermally activated jumps, needed for the continuation of the motion of the particle, are frozen out [97].

When modeling charge transport in a disordered environment, a useful concept is that of the *effective transport energy* [111–114]. This idea is derived from the concept of the *mobility edge* in an amorphous inorganic semiconductor [115, 116]. In an amorphous inorganic semiconductor, tail states are split off from the conduction and valence band. Electrons and holes are localized in those tail states and transport requires thermal activation from localized to delocalized states. The highest energy at which states are still localized defines a mobility edge [116]. In amorphous organic semiconductors, all states are localized forming a Gaussian DOS distribution, and the charge carriers reside in the tail states. Their transport requires thermal activation. If thermal excitation promotes a carrier only to a nearby site from which further jumps away are still energetically unfavorable and thus unlikely, the carrier is prone to relax back to the original site. In contrast, excitation to states closer to the center of the DOS implies a good chance to a series of subsequent jumps away from the initial site. The energy at which such transport away is enabled is called the *effective transport energy*. It is below the center of the Gaussian DOS and depends on temperature.

The Resulting Microscopic Description The disorder model can readily account for the motion of a packet of charge carriers. The following pertinent features become apparent.

Consider a charge carrier or, equivalently, a neutral exciton generated at an arbitrary site within a DOS distribution. It hops from one site to the next, thereby relaxing toward the tails of the distribution. While initially energetically downhill hops will dominate the carrier's path, eventually a balanced equilibrium between downhill and thermally activated uphill jumps will be established and a quasi-equilibrium is obtained (Figure 3.16). The mean quasi-equilibrium energy ε_∞ of the carriers is then given by the long time limit of the statistically weighted average, using the Gaussian $g(\varepsilon) = (1/\sqrt{2\pi}\sigma)\exp(-(\varepsilon - \varepsilon_0)^2/2\sigma^2)$ with $\varepsilon_0 = 0$ for the distribution function. This yields

$$\varepsilon_\infty = \lim_{t\to\infty} \varepsilon(t) = \frac{\int_{-\infty}^{+\infty} \varepsilon g(\varepsilon)\exp(-\varepsilon/kT)\mathrm{d}\varepsilon}{\int_{-\infty}^{+\infty} g(\varepsilon)\exp(-\varepsilon/kT)\mathrm{d}\varepsilon} = -\frac{\sigma^2}{kT} \tag{3.41}$$

If the mean carrier energy, relative to the center of the DOS, is normalized to its standard deviation, one can write Eq. (3.41) in the form $\varepsilon_\infty/\sigma = -[kT/\sigma]^{-1}$, that is, the disorder-normalized quasi-equilibrium energy is inversely proportional to the disorder-normalized thermal energy. As

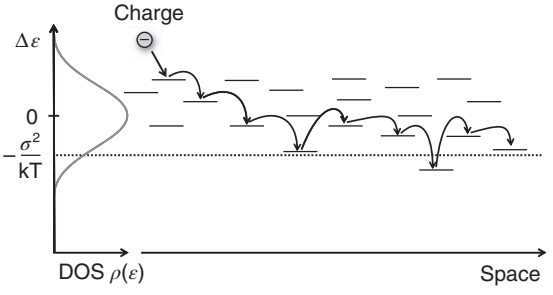

Figure 3.16 Illustration of a charge carrier, generated at an arbitrary energy, that hops within a Gaussian DOS. The dotted horizontal line is the energy at which the charge carriers tend to equilibrate in the long time limit.

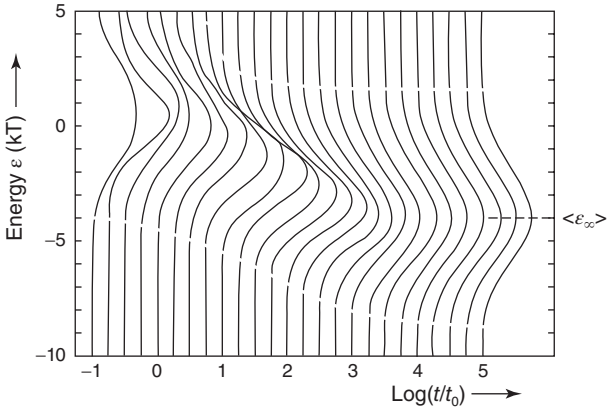

Figure 3.17 Illustration of temporal evolution of a packet of non-interacting charge carriers that relaxes within a Gaussian DOS distribution. ε_∞, in units of kT, is the energy at which quasi-equilibrium is attained. (After Bässler [99].)

the disorder model applies not only to the motion of charges but also to the motion of excitons, the temperature shift of ε_∞ can be readily observed as a temperature shift in the emission spectra (see Section 3.7.3).

Using Monte Carlo simulation or EMA calculations, one finds that the mean energetic relaxation of excitations (charges or excitons) in a Gaussian DOS follows a logarithmic decay law with respect to time, $\varepsilon(t) \propto \ln(t/t_0)$, until the equilibrium energy is reached in the long time limit (Figure 3.17). An exception to this is the very low temperature range when the motion of charge carriers becomes kinetically frozen out so that a charge gets stuck in a local energy minimum instead of reaching the lower equilibrium energy. Experimental evidence can be observed easily for excitons when considering the time dependent shift of emission spectra in a neat film as discussed in Section 3.7.3.

One consequence of the time-dependent energetic relaxation is that the diffusivity, and concomitantly the mobility of charge carriers also become time-dependent until the carriers have reached the quasi-equilibrium energy. Once that is reached, diffusivity and mobility are time-independent. As mentioned in the context of Eq. (3.1), the diffusivity is given by square of the distance traveled in a time interval divided by the time interval, $D = l^2/t$. The mobility results from the diffusivity through the Einstein relation, Eq. (3.7), $eD = \mu kT$. If a carrier is placed somewhere in the DOS, say, energetically close to the center, it will initially find many lower energy sites to jump to, thus quickly diffusing away from its initial site and covering some distance within a time interval. At later times, the carrier is surrounded by many sites of equal and few of lower energy resulting in a more randomly oriented diffusive motion that covers less total distance in a given time interval, thus leading to a reduced diffusivity compared to the early time situation. From this brief discussion, it is evident that diffusivity and mobility depend on time as well as on the initial energy of the carrier within the DOS. This is illustrated in Figure 3.18. Note that when starting at very low energies in the DOS, the carrier diffusivity may even reduce significantly before merging to the long-time quasi-equilibrium value.

As the diffusivity depends on time, temperature, and local energy landscape, the transport of an ensemble of charge carriers becomes dispersive until the quasi-equilibrium is attained (Box 3.6). This can be observed when a packet of charge carriers is generated optically in the course of a ToF experiment. Right after their generation, the charge carriers relax energetically toward quasi-equilibrium. This is revealed by the initial decay of the ToF signal that merges into a plateau indicating that the relaxation process is finished. The plateau is associated with a constant displacement current that persists until the sheet of carriers initially generated reaches the counter electrode. When lowering the temperature, the relaxation is slowed down and local variations in the diffusivity become pronounced. As a result, some carriers in the wave packet move with higher mobility, others with lower, and the

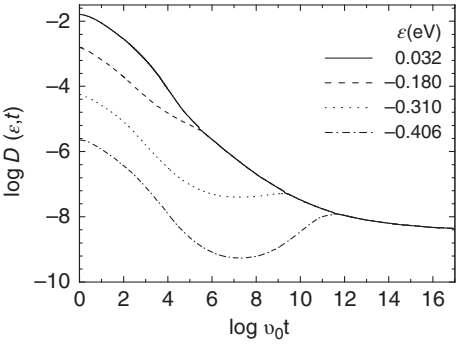

Figure 3.18 The log of the energy-and time-dependent diffusivity $D(\varepsilon, t)$ calculated by an effective medium approach for transport at 230 K in a Gaussian density of states of width $\sigma = 100$ meV and density $= 8 \times 10^{18}$ cm^{-3}. The diffusivity is calculated for different start energies. (Data from Movaghar *et al*. [97].)

overall transport becomes dispersive. The sheet of charge carriers no longer arrives at the counter electrode at a reasonably well identifiable time and the ToF signal becomes smeared out and looses its kink marking the arrival time. This typically occurs above a critical disorder parameter $\sigma/kT > 4$. This is illustrated in Figure 3.19. For an overview on ToF measurements, we refer to [117].

Box 3.6 The Continuous Time Random Walk (CTRW Model)

The continuous time random walk (CTRW) concept has been introduced by Scher and Montroll [120] to understand why charge transport in amorphous inorganic semiconductors such as chalcogenides is dispersive, that is, the velocity of an ensemble of charge carriers decreases continuously with time. In the early seventies, those materials were used as photoreceptors used in Xerography. Scher and Montroll postulated that in an amorphous system, the probability of a charge carrier to leave an occupied lattice site is not an exponential function of time but rather controlled by a broad waiting time distribution $\Psi(t) = t^{-(1+\alpha)}$, with $0 < \alpha < 1$ being a dispersion parameter. This function is introduced in a heuristic manner and is not directly related to microscopic parameters. This form of the waiting time distribution gives rise to a slowing down of the velocity of an ensemble of charge carriers. It predicts a ToF signal that features a time dependence of the photocurrent (PC) of the form

$$j(t) \propto \begin{cases} t^{-(1-\alpha)}, & t \le t_{\mathrm{tr}} \\ t^{-(1+\alpha)}, & t > t_{\mathrm{tr}} \end{cases} \qquad \text{(B3.6.1)}$$

in which t_{tr} is the effective transit time defined by the kink in the $\ln j(t)$ versus $\ln t$ dependence, and α is a dispersion parameter, In the case of an exponential distribution of hopping sites $\alpha = T/T_0$, where T_0 is the characteristic temperature of the distribution of hopping states. It is important to keep in mind, however, that the particular waiting time distribution $\Psi(t)$ chosen by Scher *et al.*, and the resulting dispersive PC is only realized in systems in which charge transport takes place via carrier jumps from an exponential distribution of localized states to an either well defined conduction band edge or to a so-called mobility edge within a distribution of hopping states [121]. The characteristic feature of transport in an exponential DOS is that a transient PC remains dispersive within the entire time regime, that is, a ToF signal never attains a plateau because quasi-equilibrium is never attained. This is at variance with experimental results on a great variety of random organic semiconductors. Historically, the need to consider disorder transport arose during the development of the xerographic process in the 1970s.

If quasi-equilibrium is established and the number of charge carriers is much less than the number of hopping sites, then the carriers occupy sites with a mean energy $-\sigma^2/kT$ relative to the center of the Gaussian DOS distribution. In this case, transport requires that charge carriers have to be thermally activated to reach the effective transport energy where transport occurs. Since the quasi-equilibrium energy decreases with temperature, the activation energy must increase accordingly. Therefore, the temperature dependence of the mobility must deviate from the Arrhenius' law and bear out a

$$\mu = \mu_0 \exp\left(-C\left(\frac{\sigma}{kT}\right)^2\right) \tag{3.42}$$

law, tacitly assuming that geometric relaxation in the course of hopping transport is unimportant. The C is a scaling parameter that takes into account that both the initial and final hopping states are distributed in energy. For a three-dimensional system, one finds $C = 0.44$ ($\approx(2/3)^2$). A representative experimental result is shown in Figure 3.20, illustrating that the mobility data fit to the exponential $1/T^2$ dependence and not to the exponential $1/T$ dependence that would be characteristic for a purely polaronic transport [122, 123]. Note, however, that in practice, it is often difficult to distinguish

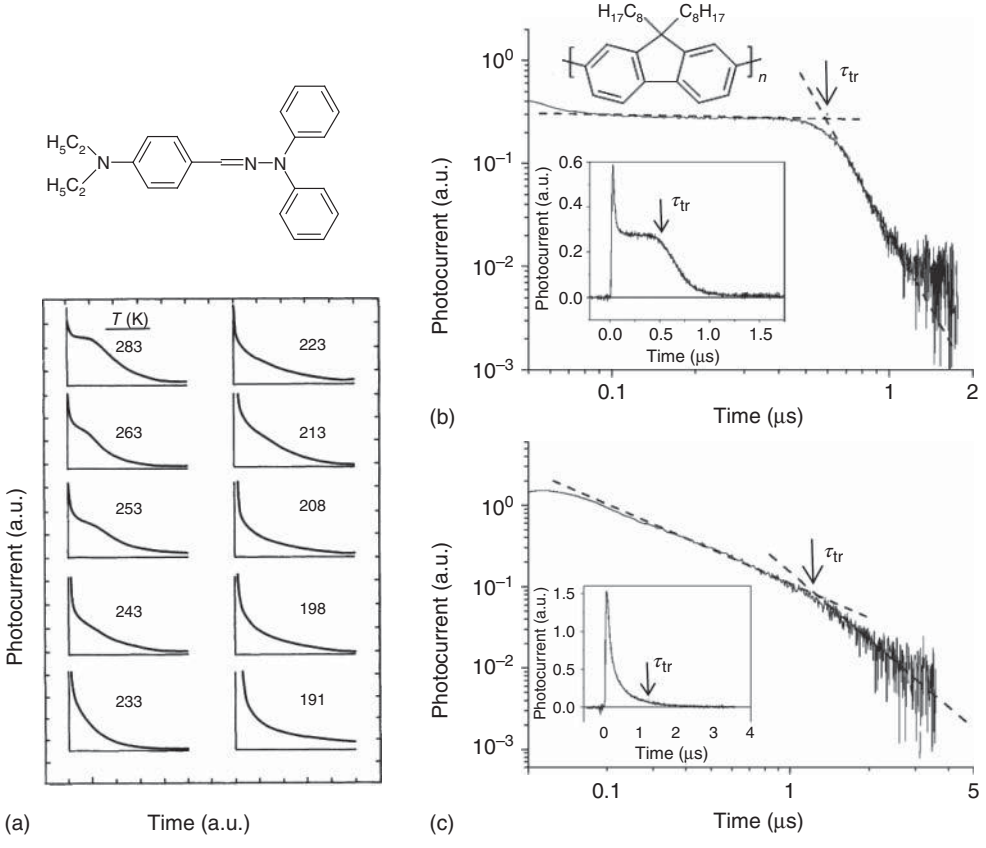

Figure 3.19 In (a) it is shown how the time of flight signal of holes migrating in glass of the molecule depicted above becomes dispersive upon cooling from 283 to 191 K. (Data from Borsenberger *et al*. [118].). In (b) and (c), the TOF-signals are shown for a 1 μm thick film of the polymer PFO depicted above that was measured at 20 V. The data are plotted on a double-logarithmic scale so that the transit time τ_{tr} can be inferred from the change of slope. The inset shows the same data on a linear scale. In (b), the film was annealed at 120 °C resulting in non-dispersive transport. In (c) the film was not annealed and the transport is dispersive. (Data for (b) and (c) from Kreouzis *et al*. [119].)